Load Adaptive PMSM Drive System Based on an Improved ADRC for Manipulator Joint

Lu, Wenqi; Li, Qiang; Lu, Kaiyuan; Lu, Yujun; Guo, Liang; Yan, Weican; Xu, Feng

Published in:
IEEE Access

DOI (link to publication from Publisher):
10.1109/ACCESS.2021.3060925

Publication date:
2021

Document Version
Publisher's PDF, also known as Version of record

IEEE Access
Multidisciplinary ⋮ Rapid Review ⋮ Open Access Journal

Received February 2, 2021, accepted February 10, 2021, date of publication February 22, 2021, date of current version March 3, 2021.

Digital Object Identifier 10.1109/ACCESS.2021.3060925

Load Adaptive PMSM Drive System Based on an Improved ADRC for Manipulator Joint

WENQI LU[1], (Member, IEEE), QIANG LI[1], KAIYUAN LU[2], (Member, IEEE), YUJUN LU[1], LIANG GUO[1], WEICAN YAN[3,4], AND FENG XU[5]

[1]Faculty of Mechanical Engineering and Automation, Zhejiang Sci-Tech University, Hangzhou 310018, China
[2]Department of Energy Technology, Aalborg University, 9220 Aalborg, Denmark
[3]College of Electrical Engineering, Zhejiang University, Hangzhou 310018, China
[4]Wolong Electric Group Company Ltd., Shaoxing 312300, China
[5]Maider Medical Industry Equipment Company Ltd., Taizhou 317600, China

Corresponding authors: Wenqi Lu (luwenqi@zstu.edu.cn) and Kaiyuan Lu (klu@et.aau.dk)

This work was supported in part by the Key Research and Development Program of Zhejiang Science and Technology Department under Grant 2021C01071, in part by the Zhejiang Provincial Natural Science Foundation of China under Grant LY18E070006 and Grant LY19E070006, in part by the National Natural Science Foundation of China under Grant 51677172, and in part by the Fundamental Research Funds of Zhejiang Sci-Tech University under Grant 2019Q031.

ABSTRACT High-speed and high-precision position servo system of permanent magnet synchronous motor (PMSM) is the key part of the research and development of the manipulator's joint. The active disturbance rejection control (ADRC) is one of the commonly used methods in the position servo system, which has the advantages of fast speed and easy physical realization. However, the existing ADRC mostly adopts the three-loop structure of position-speed-current, which has some problems such as slow positioning response, poor positioning accuracy, and poor load adaptability caused by difficult parameter tuning. Therefore, a new load adaptive two-loop drive system based on an improved position-speed integrated ADRC with a parameter fuzzy self-tuning method is proposed. In order to verify the effectiveness of the scheme, a test platform for a Selective Compliance Assembly Robot Arm (SCARA) is established. The results show that the drive system designed by the proposed method has high positioning accuracy, fast positioning response, and adaptability to load changes.

INDEX TERMS High-speed, high-precision, improved position-speed integrated ADRC, SCARA, parameter fuzzy self-tuning.

I. INTRODUCTION

With the proposal of ''Industry 4.0'', the demand for industrial robots is increasing. Selective Compliance Assembly Robot Arm (SCARA) has a large market demand in the fields of mechanical processing, medical industry, goods handling, PCB welding, etc., because of its advantages of simple structure, high repetition accuracy, and fast dynamic response. The high-speed and high-precision position servo system is one of the key components for the research and development of the SCARA. In recent years, many strategies of improving positioning response, positioning accuracy, and restraining parameter changes or disturbances are proposed, which mainly have two methods: one is the method of position-speed-current three-loop control structure [3]–[16], the other is the method of position-current two-loop control structure [17]–[24].

The first method is proposed based on the three-loop structure of position-speed-current. In [3], [4], an adaptive control strategy based on a disturbance observer is proposed. The disturbance observer is used to estimate the load change, and the adaptive controller is used to compensate for the norm bounded disturbance, which effectively improves the anti-interference ability and robustness of the system. In [5]–[7], a PMSM drive system based on the fuzzy controller is proposed. The adaptive control law of parameter uncertainty and external interference in error state space is derived, which improves the anti-interference ability of the system. In [8], [9], a nonlinear internal model control based on the output feedback controller is proposed, which can achieve exact position tracking and allow certain parameter uncertainties. The experiment proved that the proposed controller could lead to a high precision position tracking

The associate editor coordinating the review of this manuscript and approving it for publication was Shihong Ding.

performance under nonlinear load torque disturbance. In [10]–[13], a three-loop PMSM position servo system based on the sliding mode variable structure algorithm is designed, which adopts a cascade sliding mode controller and introduces an error term to change the fixed gain of the switching term into a variable gain, and it can effectively weaken the high-frequency chattering of the system. In [14]–[16], ADRC is used for vector control of PMSM. It can not only observe the internal disturbance of the system in real-time, but also observe the external disturbance of the system, and give compensation to achieve the purpose of precise control. However, the above schemes are all proposed based on the three-loop structure of position-speed-current. In practical application, it is more suitable for the six-axis manipulator, which needs trajectory control, and the cost is not sensitive. The research object of this paper is a four-axis SCARA, which is mainly used for point position control. Compared with the traditional position servo system of the six-axis manipulator, each joint of the four-axis SCARA servo system is not only limited by cost and space but also requires a higher performance of position control than speed control. And in the three-loop structure of position-speed-current, the existence of the medium speed loop is a large inertia series delay link, which affects the position control performance. It not only increases the order and debugging difficulty of the system but also limits the space to improve the response speed.

To further improve the positioning response of the system, the second improved method based on the position-current two-loop control structure is proposed. In [17], a PMSM position servo system with the position-current two-loop control structure based on traditional PID is proposed, and the step response and the trapezoid response are used to compare with the three-loop system under the same command signal and the same control object. The results show that the position dynamic response time of the two-loop system is less than that of the three-loop system, which is more suitable for the point position control. But the control parameters of this two-loop system are fixed, which is easily affected by parameter changes and external disturbances. In [18], a position-current two-loop position servo system based on sliding mode variable structure control is proposed, and the corresponding position-speed integrated sliding mode controller is designed. The results verify the effectiveness of the algorithm, but there are many sliding surfaces in the current algorithm, and the control structure is complex. Moreover, the dynamic response and chattering are contradictory and cannot be both excellent. In [19], [20], without sacrificing the anti-interference performance, the switching gain of the sliding mode control is reduced, the chattering of the system is effectively suppressed, and the dynamic response of the system is improved. In [21]–[24], a position-current two-loop position servo system based on second-order ADRC is designed, and the experimental results show that the scheme has good anti-disturbance performance and robustness. However, its parameter setting is complex and needs to be manually adjusted, which is not convenient for the actual operation of the project.

Therefore, in order to realize the high-speed and high-precision positioning of SCARA manipulator joint servo system in limited space and cost, aiming at the problem of slow positioning response and poor positioning accuracy of the traditional three closed-loop control system, a new two-loop drive system based on an improved position-speed integrated ADRC is proposed. Aiming at the problem of poor load adaptability caused by difficult parameter tuning of ADRC, a fuzzy parameter self-tuning is proposed. And the SCARA test prototype is established, and the algorithm is compared and tested based on one of the joints.

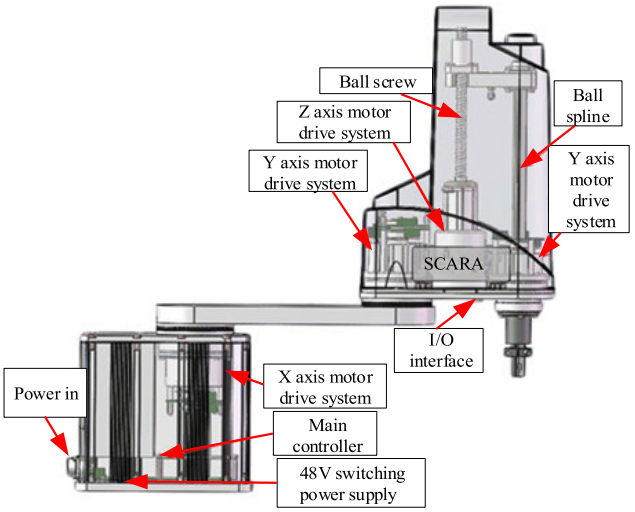

FIGURE 1. The composition and principle block diagram of the SCARA.

II. THE DESIGN OF THE PROPOSED SCARA

The composition and principle block diagram of the SCARA is designed as shown in Fig. 1. It is mainly composed of the main controller, four joint axes (X/Y/Z/R), motor drive system, 48V switch power supply, ball screw, ball spline, I/O interface, and external (power input, windpipe, signal) interface, etc. The motor drive system consists of a motor, driver, reducer, and encoder. Among them, the X/Y two revolving joints realize the rapid positioning and orientation in the plane. The Z rotation joint and the R motion joint complete the rotation and up-down motion in the vertical plane. The characteristic of the SCARA is that the motor drive system is installed in the joint module body, which is designed in a hollow manner, the main controller and the switching power are placed in the base of the joint module. Thus, the space and cost of the whole joint module are greatly reduced. The high-speed and high-precision motor drive system is one of the essential key components in the research and development of SCARA. Therefore, a new load adaptive two-loop drive system based on the improved position-speed integrated ADRC with the parameter self-tuning method is proposed, which is described in detail below.

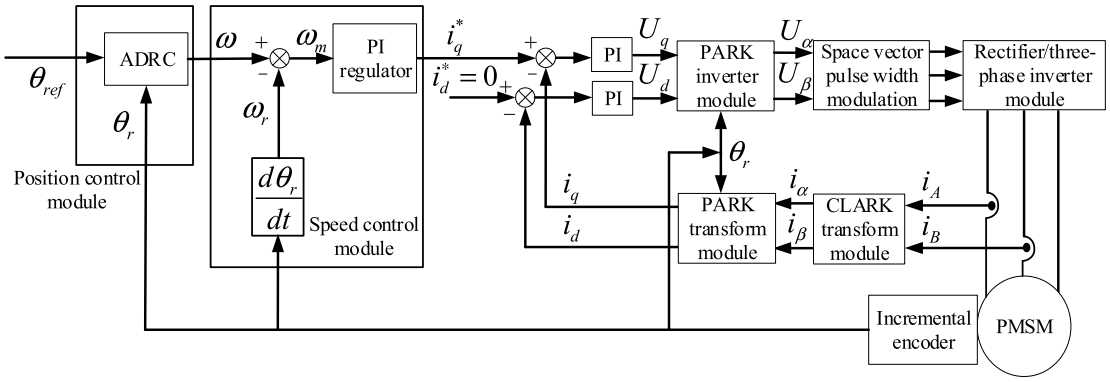

FIGURE 2. The principle block diagram of the traditional position servo system based on the traditional ADRC.

III. TRADITIONAL POSITION SERVO SYSTEM BASED ON THE TRADITIONAL ADRC

The principle block diagram of the traditional position servo system based on the traditional ADRC is shown in Fig. 2. It generally adopts the three-loop control structure of position- speed-current and taking the $id^* = 0$ control strategy, which is composed of position control module based on the traditional ADRC, speed control module based on the PI regulator, current control module based on the PI regulator, PARK transform, PARK inverter transform, CLARK transform, rectifier/three-phase inverter, incremental encoder, PMSM, and space vector pulse width modulation (SVPWM), etc.

The mechanical motion equation of PMSM in the rotor magnetic field oriented synchronous rotating coordinate system is (1).

$$J\frac{d^2\theta}{dt^2} = K_t i_q - B\frac{d\theta}{dt} - T_L \tag{1}$$

Among them, θ is the rotor position, J is the system moment of inertia, B is the damping coefficient, ω is the rotor speed, T_L is the load torque, and K_t is the torque coefficient.

The state equation of the PMSM position servo system [14] is (2).

$$\begin{cases} \dot{x}_1 = x_2 + b_0 u \\ \dot{x}_2 = \xi \\ y = x_1 \end{cases} \tag{2}$$

Among them, $x_1 = \theta$ is the state variable, $x_2 = a(t)$ is another state variable, which is extended by the external disturbance of the system $a(t)$, denoting $\dot{x}_2 = \xi$, $u = \omega$ is the control variable, and $b_0 = K_t/J$ is the system model parameter.

Based on (2), the traditional ADRC of position loop [15] can be constructed, and the principle block diagram of the position control module based on the traditional ADRC is shown in Fig. 3. It is mainly composed of tracking differentiator (TD), extended state observer (ESO), and linear state error feedback (LSEF). These three parts are shown in (3), (4), and (5) respectively.

$$\dot{\theta}_1 = -r^2(\theta_1 - \theta_{ref}) - rh\theta_1 \tag{3}$$

$$\begin{cases} e_1 = \theta_{z1} - \theta_r \\ \dot{\theta}_{z1} = \theta_{z2} - \beta_1(\theta_{z1} - \theta_r) + b_0\omega \\ \dot{\theta}_{z2} = -\beta_2(\theta_{z1} - \theta_r) \end{cases} \tag{4}$$

$$\begin{cases} e = \theta_{ref} - \theta_{z1} \\ \omega = k_p e - \dfrac{\theta_{z2}}{b_0} \end{cases} \tag{5}$$

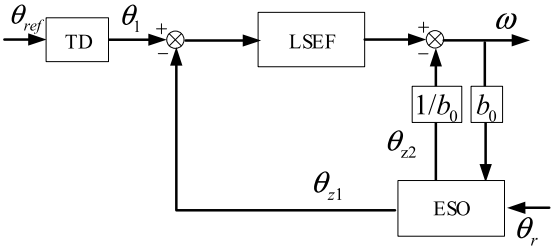

FIGURE 3. The traditional position control module based on the traditional ADRC.

Among them, θ_{ref} is the given position, θ_1 is the tracking signal, r is the tracking speed factor, h is the filtering factor, k_p is the parameter of linear proportional control, ω is the output speed of the controller, θ_r is the actual position of the motor which is obtained by encoder detection, θ_{z1} is the tracking signals of θ_r, θ_{z2} is the comprehensive disturbance value of the system expansion, including the disturbance caused by the change of load, the moment of inertia, and stator resistance, β_1 and β_2 are the gains of the ESO.

Compared with the traditional three-loop position servo system based on the PID controller, this scheme can accurately estimate and compensate for the "total disturbance" of the system [21]. However, the research object of this paper mainly focuses on point-to-point motion control, which requires the high dynamic performance of system position response, and the performance of speed regulation is relatively not high. Therefore, the speed loop in the traditional ADRC three-loop position servo system not only plays a

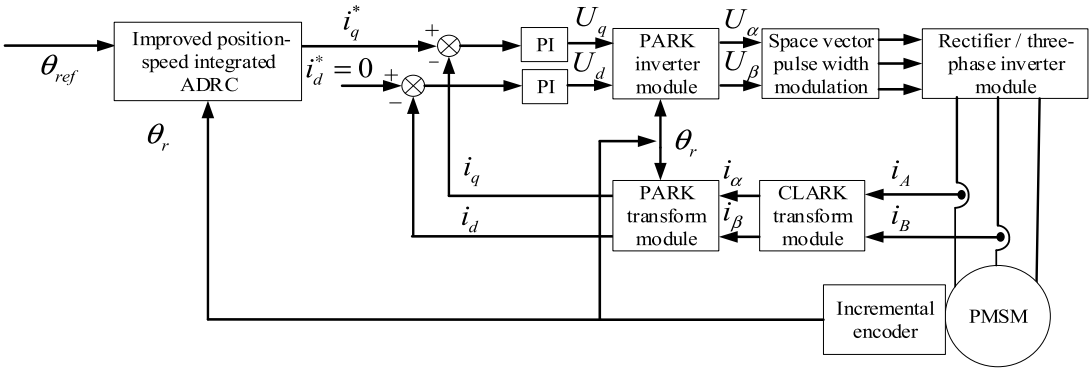

FIGURE 4. The principal block diagram of the proposed load adaptive driving system based on the proposed improved ADRC.

small role but also affects the position control performance of the system, which makes it difficult to meet the high-speed and high-precision positioning requirements. Moreover, the difficulty of parameter tuning in the traditional ADRC system not only leads to the poor load adaptability of the system but also requires continuous manual adjustment, which is not conducive to the actual operation of the project.

IV. THE PROPOSED LOAD ADAPTIVE DRIVING SYSTEM BASED ON AN IMPROVED ADRC

In order to solve the problems mentioned above, a new load adaptive two-loop drive system based on the improved position-speed integrated ADRC with the parameter self-tuning method is proposed. Its principal block diagram is shown in Fig. 4. Compared with the traditional scheme in Fig. 2, there are two improvements: The first is that the position and speed controller of the traditional position servo system is replaced by the proposed position-speed integrated controller based on the improved ADRC with a two-loop control structure. The second improvement is that the self-tuning method based on a fuzzy controller is proposed to solve the problem of parameter tuning difficulty of the ADRC.

A. THE PROPOSED POSITION-SPEED INTEGRATED CONTROLLER BASED ON THE IMPROVED ADRC

Based on the traditional state equation of the PMSM position servo system as (2), a new state equation is constructed as (6).

$$\begin{cases} \dot{x}_1 = x_2 \\ \dot{x}_2 = b_0 u + x_3 \\ \dot{x}_3 = \xi \\ y = x_1 \end{cases} \tag{6}$$

where $x_1 = \theta$ is the first state variable, $x_2 = \omega$ is the second state variable, and $x_3 = a(t)$ is the third state variable, which is extended by the external disturbance of the system $a(t)$, denote $\dot{x}_3 = \xi$, and $u = i_{q0}$ is the control variable.

Based on the new state equation (6), a new position-speed integrated controller based on the improved ADRC is proposed, and the principal block diagram is shown in Fig. 5. It is mainly composed of four parts: two-order TD, third-order

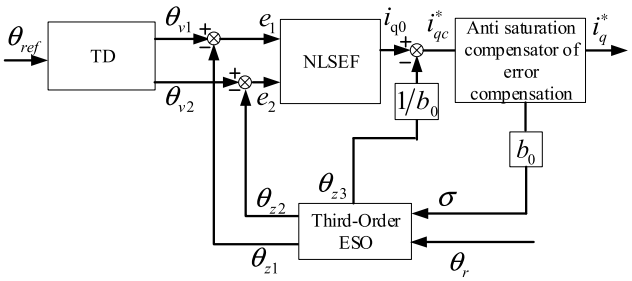

FIGURE 5. The principal block diagram of the proposed position-speed integrated controller based on the proposed improved ADRC.

ESO, nonlinear state error feedback control law (NLSEF), and anti-saturation compensator based on the error compensation. Compared with the traditional position controller based on the traditional ADRC as shown in Fig. 3. Firstly, a new TD is constructed by a second-order equation to solve the contradiction of the input signal between rapidity and overshoot; Secondly, a nonlinear function instead of a linear function is introduced to the third-order ESO to output the state variables of the system to achieve closed-loop, at the same time, the internal disturbance of the system is observed to compensate the disturbance; Thirdly, a new NLSEF is also designed based on the nonlinear function to reduce the steady-state error; Finally, an anti-saturation compensator is designed to solve the problem of control delay caused by system saturation. The final output of the position-speed integrated controller is the reference current of the q axis stator current i_q^*, not ω.

1) TWO-ORDER TD

Firstly, in order to solve the contradiction between rapidity and overshoot in control, a new formula of the two-order TD is constructed as follows.

$$\begin{cases} \dot{\theta}_{v2} = r^2 \left(\theta_{ref} - \theta_{v1}\right) - rh \cdot \theta_{v2} \\ \dot{\theta}_{v1} = \theta_{v2} \end{cases} \tag{7}$$

Among them, θ_{v1} is the tracking signal of θ_{ref} and θ_{v2} is the differential signal of θ_{v1}. By selecting such a suitable

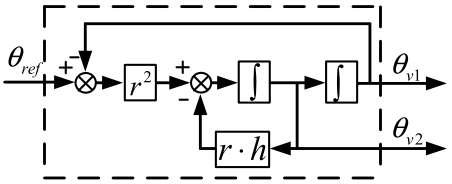

FIGURE 6. Two-Order TD.

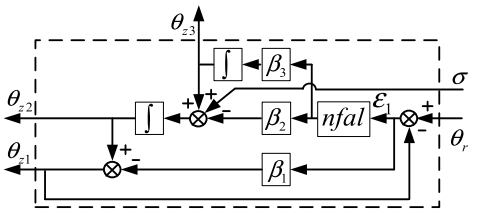

FIGURE 7. Third-order ESO.

transition process, the system can track the output of the transition process instead of directly tracking the given value of the system, so that the system can get a smoother input signal.

2) THIRD-ORDER ESO

Secondly, in order to make the system get better anti-interference ability and higher control precision, a nonlinear function is introduced to the third-order ESO, which is designed as (8).

$$nfal(e,\alpha,\delta) = \begin{cases} m_1 e + m_2 e^2 + m_3 \tan e, |e| \le \delta \\ |e|^{\alpha}\, sign(x), |e| > \delta \end{cases} \tag{8}$$

where m_1, m_2, and m_3 are the linear factor of the function, e is the input error variable of the system, δ is the filter factor, α is the nonlinear factor. In order to ensure that the function has good smoothness and avoid the phenomenon of high-frequency tremor, the nonlinear function must be continuous and differentiable at the point $e = \pm\delta$, which satisfies the condition of $f(x)_+ = f(x)_-, f(x)'_+ = f(x)'_-$, that is to satisfy the (9).

$$\begin{cases} nfal\,(e,\alpha,\delta) = \delta^{\alpha}, e = \delta \\ nfal\,(e,\alpha,\delta) = -\delta^{\alpha}, e = -\delta \\ nfal'\,(e,\alpha,\delta) = \alpha\delta^{\alpha-1}, e = \pm\delta \end{cases} \tag{9}$$

Based on (9), m_1, m_2, and m_3 can be obtained as follows.

$$\begin{cases} m_1 = \dfrac{\delta^{\alpha} + \delta^{\alpha}\tan^2\delta - \alpha\delta^{\alpha}\tan\delta}{\delta - \tan\delta + \delta\tan^2\delta} \\ m_2 = 0 \\ m_3 = \dfrac{\alpha\delta^{\alpha+1} - \delta^{\alpha}}{\delta - \tan\delta + \delta\tan^2\delta} \end{cases} \tag{10}$$

Based on the mechanical motion equation of PMSM (1), it can be rewritten as follows:

$$\frac{d^2\theta}{dt} = f_p + b_0 i_{q0} \tag{11}$$

f_p is the total disturbance of the position loop. The expression is as follows:

$$f_p = -\frac{B}{J}\frac{d\theta}{dt} + \frac{K_t}{J}i_q - \frac{T_l}{J} - b_0 i_{q0} \tag{12}$$

Therefore, combined with the (6), the formula of the third-order ESO based on the nonlinear function is constructed as (13), and its structure is shown in Fig. 7.

$$\begin{cases} \varepsilon_1 = \theta_{fdb} - \theta_{z1} \\ \dot{\theta}_{z1} = \theta_{z2} - \beta_1\varepsilon_1 \\ \dot{\theta}_{z2} = \theta_{z3} - \beta_2\, nfal\,(\varepsilon_1,\alpha_1,\delta_1) + \sigma \\ \dot{\theta}_{z3} = \beta_3\, nfal\,(\varepsilon_1,\alpha_1,\delta_1) \end{cases} \tag{13}$$

Among them, θ_{z1}, θ_{z2}, and θ_{z3} are observations of θ_r, $\dot{\theta}_r$, and f_p, ε_1 is the position angle tracking error variable, σ is the differential signal output by the anti-saturation module, which is used as a part of the system interference to compensate for the position difference signal.

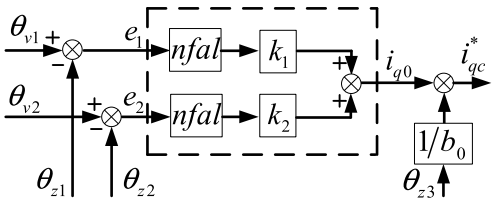

FIGURE 8. NLSEF.

3) NONLINEAR STATE ERROR FEEDBACK CONTROL LAW

Thirdly, according to transitional signals arranged by TD and output signals observed by ESO, a new NLSEF (as shown in Fig. 8) based on the nonlinear function is constructed as (14), which is to control the q axis stator current and compensate disturbance.

$$\begin{cases} e_1 = \theta_{v1} - \theta_{z1} \\ e_2 = \theta_{v2} - \theta_{z2} \\ i_{q0} = k_1 nfal\,(e_1,\alpha_2,\delta_2) + k_2\, nfal\,(e_2,\alpha_3,\delta_2) \\ i^*_{qc} = i_{q0} - \dfrac{\theta_{z3}}{b_0} \end{cases} \tag{14}$$

where θ_{v1} is the tracking signal of the system input, θ_{v2} is the differential signal of the tracking signal θ_{v1}, and k_1, k_2 are the control parameters of the NLSEF.

4) ANTI-SATURATION COMPENSATOR SCHEME BASED ON ERROR COMPENSATION

Finally, Due to the saturation phenomenon, the final feedback variable back to the third-order ESO is not the actual controller quantity. Therefore, in order to solve the problem of control lag and long regulation time caused by system saturation, an anti-saturation compensator based on error

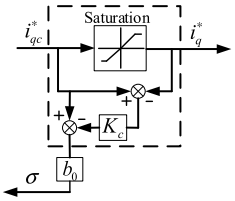

FIGURE 9. Anti-saturation compensator based on error compensation.

compensation is proposed, which is shown in Fig. 9. The input and output errors of the saturation link are amplified proportionally, and the error signal σ is fed back to the ESO as a part of the tracking error signal to compensate. The formula is designed as shown in (15).

$$\sigma = b_0(i_{qc}^* - K_c(i_{qc}^* - i_q^*)) \tag{15}$$

where i_q^* is the output current of the controller, and K_c is the anti-saturation compensation coefficient.

5) STABILITY ANALYSIS

From the state equation of the system (6) and the ESO (13), it can be concluded that the error equation of the ESO is (16).

$$\begin{cases} \varepsilon_1 = \theta_{z1} - y \\ \varepsilon_2 = \theta_{z2} - x_2 \\ \varepsilon_3 = \theta_{z3} - x_3 \\ \dot{\varepsilon}_1 = \varepsilon_2 - \beta_1\varepsilon_1 \\ \dot{\varepsilon}_2 = \varepsilon_3 - \beta_2 F_1\varepsilon_1 \\ \dot{\varepsilon}_3 = -\beta_3 F_2\varepsilon_1 \end{cases} \tag{16}$$

where $F_1 = nfal(\varepsilon_1, a, \delta)/\varepsilon_1$ and $F_2 = nfal(\varepsilon_1, a, \delta)/\varepsilon_1$. $F_1 > 0$ and $F_2 > 0$ always holds because of the same sign of nonlinear function $nfal(\cdot)$ and error variable ε_1. According to the error equation (16), $\dddot{\varepsilon}_1 + \beta_1\ddot{\varepsilon}_1 + \beta_2 F_1\dot{\varepsilon}_1 + \beta_3 F_2\varepsilon_1 = 0$ can be obtained, whose characteristic equation is $s^3 + \beta_1 s^2 + \beta_2 F_1 s + \beta_3 F_2 = 0$. Therefore, according to the Routh criterion, the stability condition can be obtained as $\beta_1 > 0$, $\beta_2 > 0$, $\beta_3 > 0$, and $\beta_1\beta_2 > \beta_3$.

B. A SELF-TUNING METHOD BASED ON THE FUZZY CONTROLLER

In the actual operation process of the system, the parameters k_1 and k_2 of the NLSEF need to be manually adjusted, which is not only complex but also not convenient for the actual operation of the project. Therefore, a self-tuning method based on the fuzzy controller is proposed.

1) STRUCTURE OF THE PARAMETER FUZZY SELF-TUNING

The structure of the proposed parameter fuzzy self-tuning is designed as shown in Fig. 10. The state errors e_1 and e_2 are taken as the input of the fuzzy controller, the correction k_1 and k_2 are taken as the output of the fuzzy controller to meet the actual requirements of the system.

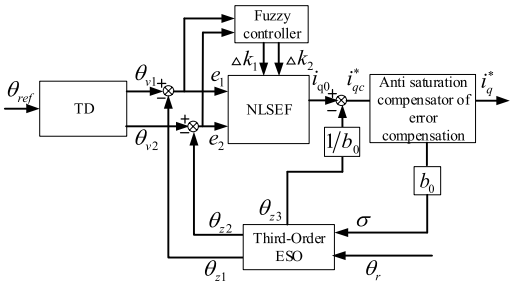

FIGURE 10. The principal block diagram of the proposed parameter self-tuning method based on the fuzzy controller.

2) LINGUISTIC VARIABLES AND MEMBERSHIP FORMULA OF LINGUISTIC TERMS

The quantization factor K_e of input error fuzzification is designed as follows.

$$K_e = n/x_e \tag{17}$$

Among them, x_e is the critical value of the basic universe of input error, n is a series of discrete input errors over the universe. The fuzzy subset is divided into {NB, NM, NS, ZO, PS, PM, PB}, and the input and output membership formula uses the triangular membership formula as follows.

$$\mu_A(x) = \begin{cases} \dfrac{x-a}{b-a} & a \le x < b \\ \dfrac{a-c}{b-c} & b \le x < c \\ 0 & x < a,\ x \ge c \end{cases} \tag{18}$$

where a, b, and c are the abscissa of the three points of the triangle on the universe.

3) DETERMINE FUZZY CONTROL RULE AND FUZZY OUTPUT

Based on the Mamdani theory and experience in engineering commissioning, such as when the position error e_1 is small, increase k_1 appropriately to enhance the anti-disturbance performance of the system; When the position error e_1 is large, increase k_2 appropriately to increase the system response; When the speed error e_2 is too large and the differential saturation causes overshoot, k_2 should be appropriately reduced; When the input error e_1 and error change rate e_2 are moderate, the appropriate k_1 and k_2 should be taken to speed up the response of the system. So the fuzzy control rules of the output variables k_1 and k_2 are designed as shown in Table 1 and Table 2. After defuzzification, the final control parameters k_1 and k_2 of the NLSEF can be calculated by fuzzy control rules and (19).

$$\begin{cases} k_1 = k_{10} + \Delta k_1 \\ k_2 = k_{20} + \Delta k_2 \end{cases} \tag{19}$$

where k_{10} and k_{20} are the initial values of k_1 and k_2 respectively.

TABLE 1. Fuzzy rule table of Δk_1.

e_1 \ e_2	NB	NM	NS	ZO	PS	PM	PB
NB	PB	PB	PM	PM	PS	PS	ZO
NM	PM	PM	PS	PS	PS	ZO	NS
NS	PS	PS	PS	PS	PS	NS	NM
ZO	PB	PM	PS	ZO	PS	PM	PB
PS	NM	NS	PS	PS	PS	PS	PS
PM	NS	ZO	PS	PS	PS	PM	PM
PB	ZO	PS	PS	PM	PM	PB	PB

TABLE 2. Fuzzy rule table of Δk_2.

e_1 \ e_2	NB	NM	NS	ZO	PS	PM	PB
NB	PB	PB	PM	PM	NS	NM	NB
NM	PB	PB	PM	PS	ZO	NS	NM
NS	PB	PB	PM	PM	PS	NS	NB
ZO	PB	PM	PS	PS	PS	PM	PB
PS	NB	NS	PS	PM	PM	PB	PB
PM	NM	NS	ZO	PS	PM	PB	PB
PB	NB	NM	NS	PM	PM	PB	PB

V. EXPERIMENT AND ANALYSIS

In order to verify the effectiveness of the proposed scheme, the key components of the SCARA are designed, such as the ordinary incremental encoder, driver, main controller, etc. The principle block diagram of the hardware scheme for the PMSM AC servo system designed is shown in Fig. 11. It mainly includes a power conversion module, a drive circuit module, the main control chip of TMS320F28335, a communication module, a position detection module, and a PWM drive module, etc.

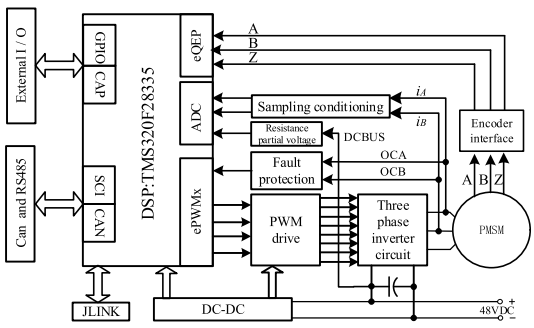

FIGURE 11. The principle block diagram of hardware scheme for PMSM AC servo system.

The main interrupt program flow chart designed is shown in Fig. 12. In the interrupt service program, the position, speed, total disturbance, and other information of the joint rotor of the manipulator are calculated by the third-order ESO and the d-q axis current are calculated by ADC sampling. The d-q axis voltage of the final stator is obtained through Fuzzy-ADRC and current loop PI to achieve closed-loop control regulation. Then after Park inverse transformation, it is sent to the SVPWM module program, and the PWM

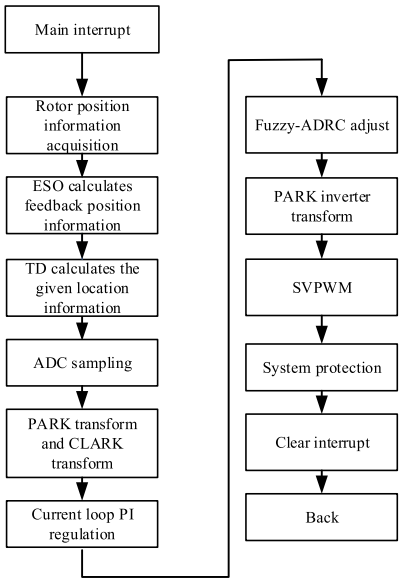

FIGURE 12. The program flow chart of the system main interrupts.

signal is output to the power module to realize the control of the mechanical arm joint. The Code Composer Studio v6.1 issued by the Texas Instruments company is used for programming.

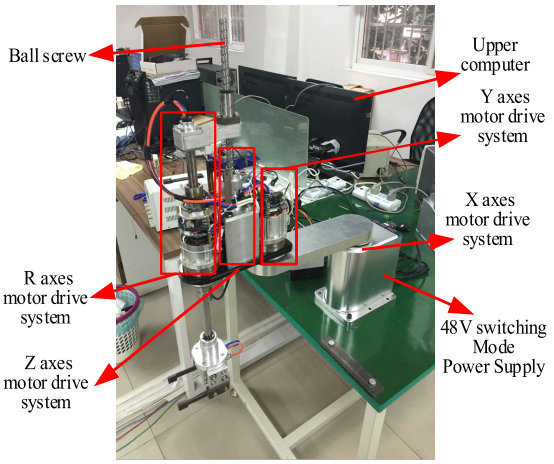

FIGURE 13. The whole machine of the SCARA for experiment platform.

The whole machine of the SCARA is designed as an experimental platform, as shown in Fig. 13. And the key parameters of the experimental platform are shown in Table 3.

A. THE TEST OF THE POSITIONING PERFORMANCE OF THE IMPROVED ADRC

In order to verify the effectiveness of the improved position-speed integrated ADRC, the comparison test is carried out with the traditional position-speed-current three-loop ADRC system when the given pulse is 5000, 10000, and 20000 respectively, and the rated load is applied.

TABLE 3. Drive system parameters.

PMSM parameters		Other key parameters	
Rated torque	0.32 N.m	Power supply voltage	48 V
Rated speed	3000 rpm	Speed measurement error	<0.05%
Rated current	4 A	Number of encoder lines	2000
Pole	6 pairs	Gear backlash	18 arcsec
Back EMF coefficient	4.3 V/rpm	Backlash of reducer	1.5 arcmin
Moment of inertia	0.02283 kg.m^2	Speed ratio of reducer	80
Inductors	0.0055 mH		
Resistance	0.3 Ω		

When the given pulse is between 0-5000 pulses, the actual position, the actual speed, the given and actual d-q axis stator current waveforms of the improved position-speed integrated ADRC system (abbreviated as IS), the actual position, the actual speed, the given and actual d-q axis stator current waveforms of the traditional position-speed-current three-loop ADRC system (abbreviated as TS) are shown in Fig. 14. According to the experimental waveform, it can be seen that when the system is running at no-load, the time for the TS motor to rise to the given pulse is 0.5 s (the descending process is 0.48 s), the actual current of the q axis follow the given q axis stator current decreased from 12.25 A to 0 A after 0.5 s, the actual current of the d axis fluctuates between −0.5 A and 0.5 A, the maximum speed of the motor is 870 r/min, and the positioning error is 0 pulse. But the time for the IS motor to rise to the given pulse is 0.4 s (the descending process is 0.38 s), the actual current of the q axis follow the given q axis stator current decreased from 12.2 A to 0 A after 0.4 s, the actual current of the d axis fluctuates between −0.5 A and 0.5 A, the maximum speed of the motor is 900 r/min, and the positioning error is 0 pulse. Therefore, compared with the TS, the IS has a faster positioning response in both ascending and descending processes. When the load of 0.32 N.m is applied at 9 s, the time for the motor of the IS to rise to the given pulse becomes long to 0.44 s (the descending process is 0.43 s), the actual current of the q axis follow the given q axis stator current decreased from 12.2 A to 4 A after 0.44 s, the actual current of the d axis fluctuates between −0.5 A and 0.5 A, the maximum speed of the motor is 850 r/min, and the positioning error becomes large, which is about 3 pulses. But the time for the TS motor to rise to the given pulse becomes longer, which is 0.55 s (the descent process is 0.54 s), the actual current of the q axis follow the given q axis stator current decreased from 12.2 A to 4 A after 0.55 s, the actual current of the d axis fluctuates between −0.5 A and 0.5 A, the maximum speed of the motor is 800 r/min, the error between the actual position and the given position becomes larger (the error is 5 pulses). Therefore, the actual q axis stator current of IS can follow the given q axis stator current faster than TS in the case of no-load or emergency load. And the positioning response of the IS is faster than that of the TS in the process of sudden load loading, but the position error also increases.

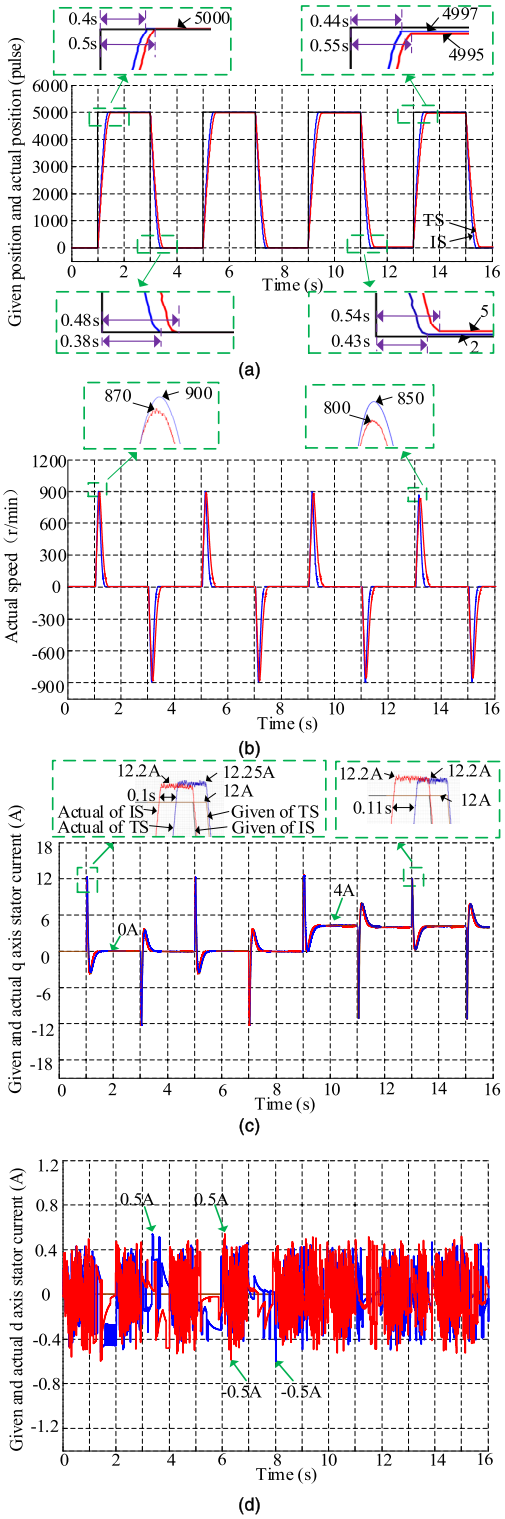

FIGURE 14. Comparison test of the TS and the IS when the given pulse is 5000. (a) The actual position of the TS and the IS. (b) The actual speed of the TS and the IS. (c) The given and actual q axis stator current of the TS and the IS. (d) The given and actual d axis stator current of the TS and the IS.

When the given pulse is between 0-10000 pulse, the actual position and speed waveforms of the IS and the TS, the given and actual d-q axis stator current of the TS and the IS are shown in Fig. 15. According to the experimental waveform, it can be seen that when the system is running at no-load, the time for the TS motor to rise to the given pulse is 0.75 s (the descending process is 0.73 s), the actual current of the q axis follow the given q axis stator current decreased from 12.2 A to 0 A after 0.75 s, the actual current of the d axis fluctuates between −0.5 A and 0.5 A, the maximum speed of the motor is 1130 r/min, and the positioning error is 2 pulses. But the time for the IS motor to rise to the given pulse is 0.6 s (the descending process is 0.57 s), the actual current of the q axis follow the given q axis stator current decreased from 12.2 A to 0 A after 0.6 s, the actual current of the d axis fluctuates between −0.5 A and 0.5 A, the maximum speed of the motor is 1150 r/min, and the positioning error is 1 pulse. Therefore, compared with the TS, the IS has a faster positioning response in both ascending and descending processes. When the load of 0.32 N.m is applied at 9 s, the time for the motor of the IS to rise to the given pulse becomes long to 0.67 s (the descending process is 0.65 s), the given current of the q axis follow the given q axis stator current decreased from 12 A to 4 A after 0.67 s, the actual current of the d axis fluctuates between −0.5 A and 0.5 A, the maximum speed of the motor is 1100 r/min, and the positioning error becomes large to 4 pulses. But the time for the TS motor to rise to the given pulse becomes longer to 0.83 s (the descent process is 0.82 s), the given current of the q axis follow the given q axis stator current decreased from 12 A to 4 A after 0.83 s, the actual current of the d axis fluctuates between −0.5 A and 0.5 A, the maximum speed of the motor is 1050 r/min, the error between the actual position and the given position becomes larger (the error is 20 pulses). Therefore, the actual q axis stator current of IS can follow the given q axis stator current faster than TS in the case of no-load or emergency load. And the positioning response of the IS is faster than that of the TS in the process of sudden load loading, but the positioning error also appears.

When the given pulse is between 0-20000 pulses, the actual position and actual speed waveforms of the IS and the TS, the given and actual d-q axis stator current of the TS and the IS are shown in Fig. 16. According to the experimental waveform, it can be seen that when the system is running at no-load, the time for the TS motor to rise to the given pulse is 0.9 s (the descending process is 0.89 s), the actual current of the q axis follow the given q axis stator current decreased from 12 A to 0 A after 0.9 s, the actual current of the d axis fluctuates between −0.5 A and 0.5 A, the maximum speed of the motor is 2050 r/min, and the positioning error is 2 pulses. But the time for the IS motor to rise to the given pulse is 0.82 s (the descending process is 0.8 s), the actual current of the q axis follow the given q axis stator current decreased from 12 A to 0 A after 0.82 s, the actual current of the d axis fluctuates between −0.5 A and 0.5 A, the maximum speed of the motor is 2100 r/min, the positioning error is 2 pulses. Therefore,

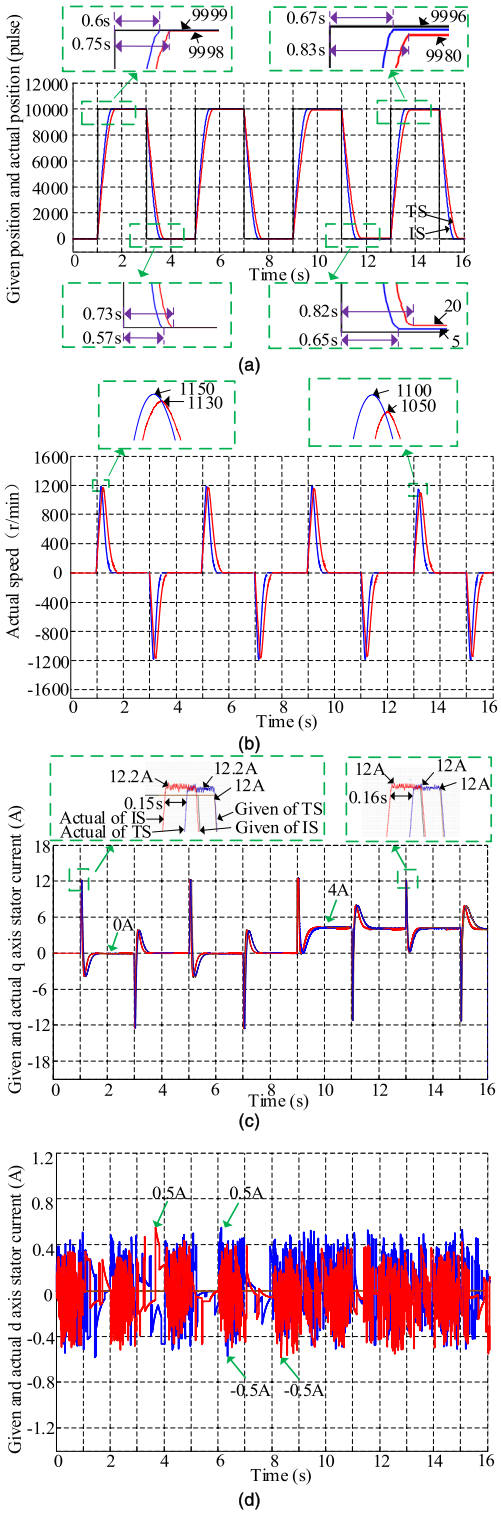

FIGURE 15. Comparison test of the TS and the IS when the given pulse is 10000. (a) The actual position of the TS and the IS. (b) The actual speed of the TS and the IS. (c) The given and actual q axis stator current of the TS and the IS. (d) The given and actual d axis stator current of the TS and the IS.

compared with the TS, the IS has a faster positioning response in both ascending and descending processes. When the load of 0.32 N.m is applied at 9 s, the time for the motor of

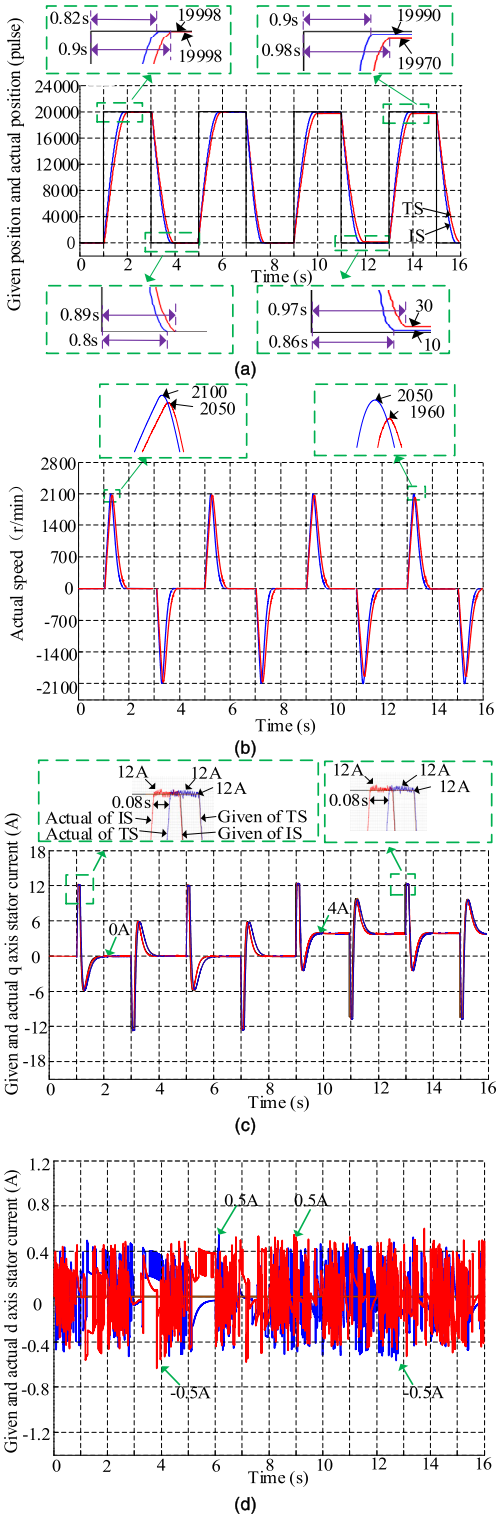

FIGURE 16. Comparison test of the TS and the IS when the given pulse is 20000. (a) The actual position of the TS and the IS. (b) The actual speed of the TS and the IS. (c) The given and actual q axis stator current of the TS and the IS. (d) The given and actual d axis stator current of the TS and the IS.

the IS to rise to the given pulse becomes long to 0.9 s (the descending process is 0.86 s), the actual current of the q axis follow the given q axis stator current decreased from 12 A to 4 A after 0.9 s, the actual current of the d axis fluctuates between −0.5 A and 0.5 A, the maximum speed of the motor is 2050 r/min, and the positioning error becomes large to 10 pulses. But the time for the TS motor to rise to the given pulse becomes longer to 0.98 s (the descent process is 0.97 s), the actual current of the q axis follow the given q axis stator current decreased from 12 A to 4 A after 0.98 s, the actual current of the d axis fluctuates between −0.5 A and 0.5 A, the maximum speed of the motor is 1960 r/min, the error between the actual position and the given position becomes larger (the error is 30 pulses). Therefore, the actual q axis stator current of IS can follow the given q axis stator current faster than TS in the case of no-load or emergency load. And the positioning response of the IS is faster than that of the TS in the process of sudden load loading, but the positioning error also appears.

Therefore, based on the above experimental results, it can be seen that when the system is running at no-load, the positioning errors of the IS and the TS are both ±2 pulses, but the positioning response of the IS is faster than that of the TS. Whereas in the process of sudden load increase, the IS has a faster positioning response, but it also has the situation of a larger positioning error, which does not meet the requirements of high-precision positioning of the manipulator.

B. THE TEST OF THE POSITIONING PERFORMANCE OF THE IMPROVED ADRC WITH PARAMETER FUZZY SELF-TUNING

In order to verify the effectiveness of the proposed fuzzy controller, based on the proposed position-speed integrated ADRC, the effectiveness of the proposed method based on fuzzy self-tuning is verified, when the given pulse is 5000, 10000, and 20000 respectively, and the rated load is applied.

When the given pulse is between 0-5000 pulses, the actual position, actual speed, and the given actual d-q axis stator current waveforms of the IS and the improved position-speed integrated ADRC system with fuzzy controller parameter self-tuning (abbreviated as FS) are shown in Fig. 17. According to the experimental waveform, it can be seen that when the system is running without load, the time for the IS and the FS motors to rise to the given pulse is 0.4 s (the descent process is 0.38 s), the actual current of the q axis follow the given q axis stator current decreased from 12.2 A to 0 A after 0.4 s, the actual current of the d axis fluctuates between −0.5 A and 0.5 A, the maximum speed of the motor is 900 r/min, and the positioning error is 0 pulse. When the load of 0.32 N.m is applied at 9 s, the maximum speed of the IS motor decreases 50 r/min, and the time of motor rising to the given pulse becomes long to 0.44 s (the descending process is 0.43 s), the actual current of the q axis follow the given q axis stator current decreased from 12.2 A to 4 A after 0.44 s, the actual current of the d axis fluctuates between −0.5 A and 0.5 A, the positioning error becomes large to 3 pulses. However, the maximum speed of the FS motor is almost constant, and the time of the motor rising to the given pulse is only increased to 0.41 s (the descent

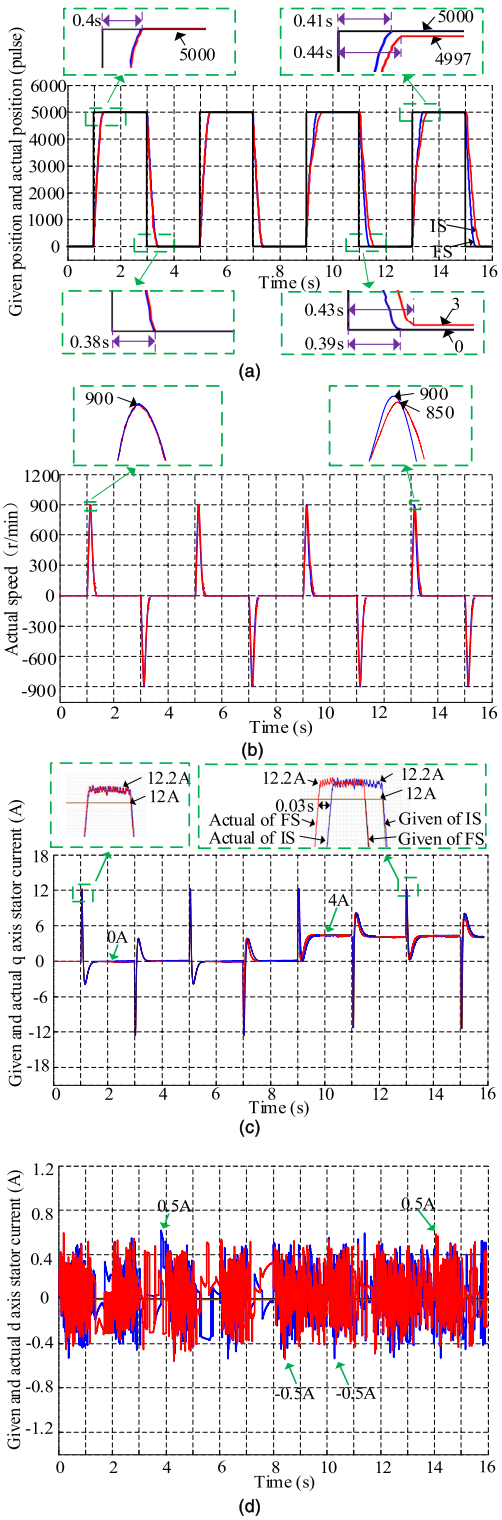

FIGURE 17. Comparison test of the IS and the FS when the given pulse is 5000. (a) The actual position of the IS and the FS. (b) The actual speed of the IS and the FS. (c) The given and actual q axis stator current of the IS and the FS. (d) The given and actual d axis stator current of the IS and the FS.

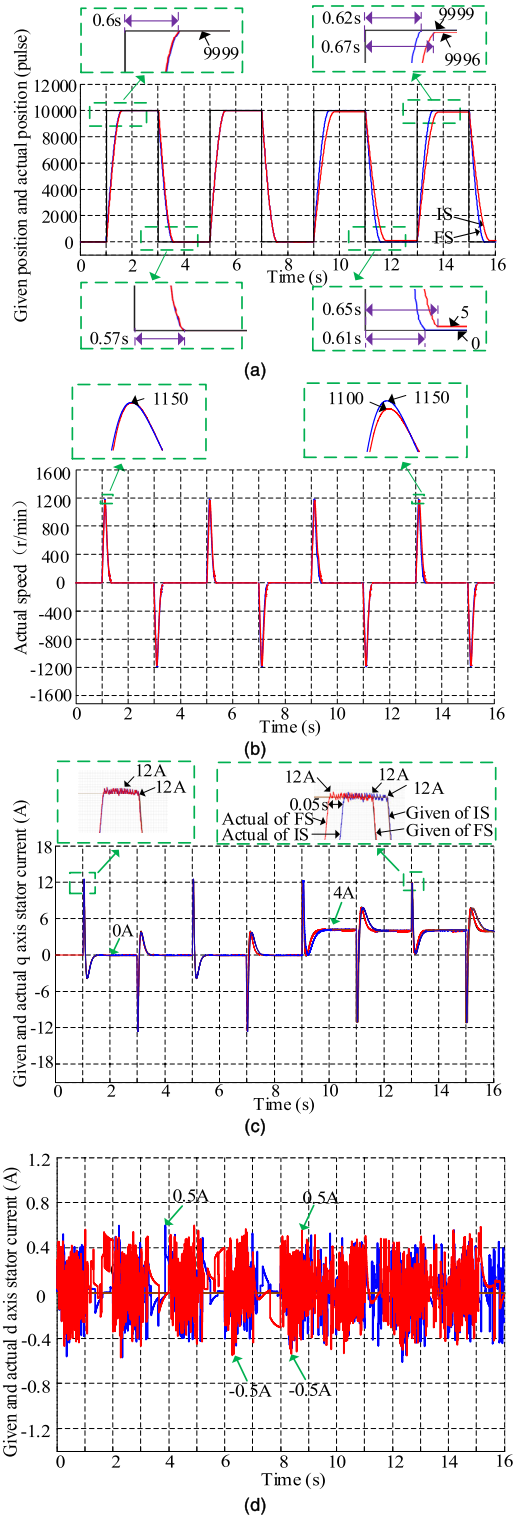

FIGURE 18. Comparison test of the IS and the FS when the given pulse is 10000. (a) The actual position of the IS and the FS. (b) The actual speed of the IS and the FS. (c)The given and actual q axis stator current of the IS and the FS. (d)The given and actual d axis stator current of the IS and the FS.

process is 0.39 s), the actual current of the q axis follow the given q axis stator current decreased from 12.2 A to 4 A after 0.41 s, the actual current of the d axis fluctuates between −0.5 A and 0.5 A, the positioning error is still within 0 pulses. Therefore, the actual q axisstator current of FS can follow the given q axis stator current faster than IS in the case of

no-load or emergency load. And in the process of sudden load increase, the improved system based on parameter fuzzy self-tuning has higher positioning accuracy and faster positioning response.

When the given pulse is between 0-10000 pulses, the actual position and actual speed waveforms of the IS and the TS, and the given and actual d-q axis stator current of the IS and the FS are shown in Fig. 18. According to the experimental waveform, it can be seen that when the system is running without load, the time for the IS and the FS motors to rise to the given pulse is 0.6 s (the descent process is 0.57 s), the actual current of the q axis follow the given q axis stator current decreased from 12 A to 0 A after 0.6 s, the actual current of the d axis fluctuates between −0.5 A and 0.5 A, the maximum speed of the motor is 1150 r/min, and the positioning error is 0 pulse. When the load of 0.32 N.m is applied at 9 s, the maximum speed of the IS motor decreases 50 r/min, and the time of motor rising to the given pulse becomes long to 0.67 s (the descending process is 0.65 s), the actual current of q axis follow the given q axis stator current decreased from 12 A to 4 A after 0.67 s, the actual current of the d axis fluctuates between −0.5 A and 0.5 A, the positioning error becomes large to 5 pulses. However, the maximum speed of the FS motor is almost constant, and the time of the motor rising to the given pulse is only increased to 0.62 s (the descent process is 0.61 s), the actual current of the q axis follow the given q axis stator current decreased from 12 A to 4 A after 0.62 s, the actual current of the d axis fluctuates between −0.5 A and 0.5 A, the positioning error is still within ±1 pulse. Therefore, the actual q axis stator current of FS can follow the given q axis stator current faster than IS in the case of no-load or emergency load. And in the process of sudden load increase, the improved system based on parameter fuzzy self-tuning has higher positioning accuracy and faster positioning response.

When the given pulse is between 0-20000 pulses, the actual position and actual speed waveforms of the IS and the TS, and the given and actual d-q axis stator current of the IS and the FS are shown in Fig. 19. According to the experimental waveforms, it can be seen that when the system is running without load, the time for the IS and the FS motors to rise to the given pulse is 0.82 s (the descent process is 0.8 s), the actual current of the q axis follow the given q axis stator current decreased from 12 A to 0 A after 0.82 s, the actual current of the d axis fluctuates between −0.5 A and 0.5 A, the maximum speed of the motor is 2100 r/min, and the positioning error is 1 pulse. When the load of 0.32 N.m is applied at 9 s, the maximum speed of the IS motor decreases 50 r/min, and the time of the motor rising to the given pulse becomes long to 0.9 s (the process is 0.86 s), the actual current of the q axis follow the given q axis stator current decreased from 12 A to 4 A after 0.9 s, the actual current of the d axis fluctuates between −0.5 A and 0.5 A, the positioning error becomes large to 10 pulses. However, the maximum speed of the FS motor is almost constant, and the time of the motor rising to the given pulse is only increased to 0.83 s

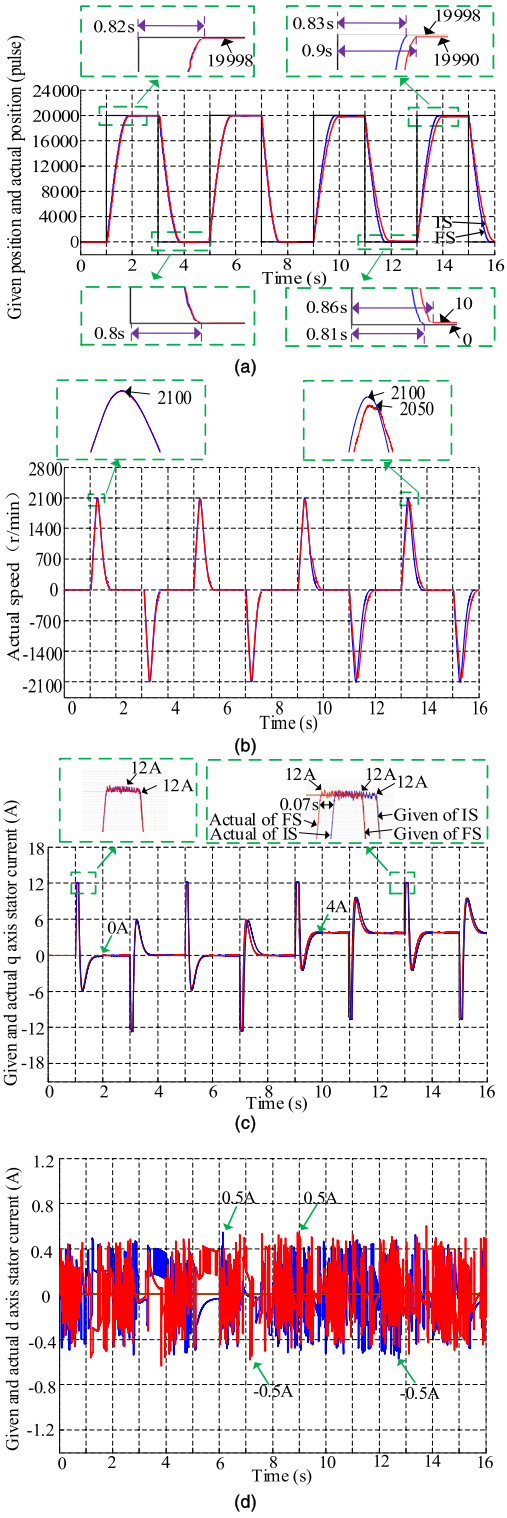

FIGURE 19. Comparison test of the IS and the FS when the given pulse is 20000. (a) The actual position of the IS and the FS. (b) The actual speed of the IS and the FS. (c) The given and actual q axis stator current of the IS and the FS. (d)The given and actual d axis stator current of the IS and the FS.

(the descent process is 0.81 s), the actual current of the q axis follow the given q axis stator current decreased from 12 A to 4 A after 0.83 s, the actual current of the d axis

fluctuates between −0.5 A and 0.5 A, the positioning error is still within ±2 pulses. Therefore, the actual q axis stator current of FS can follow the given q axis stator current faster than IS in the case of no-load or emergency load. And in the process of sudden load increase, the improved system based on parameter fuzzy self-tuning has higher positioning accuracy and faster positioning response.

Therefore, according to the above experimental results, in the process of sudden load increase, the introduction of parameter fuzzy self-tuning link reduces the dynamic speed drop of the system, effectively suppresses the impact of load disturbance and improves the positioning response and positioning accuracy of the system.

C. THE TEST OF PARAMETER CHANGES

The main parameters that affect the performance of the proposed method are the resistance, inductance, and mechanical inertia of the motor. And the influence of three parameters changes is analyzed based on the modelling and simulation.

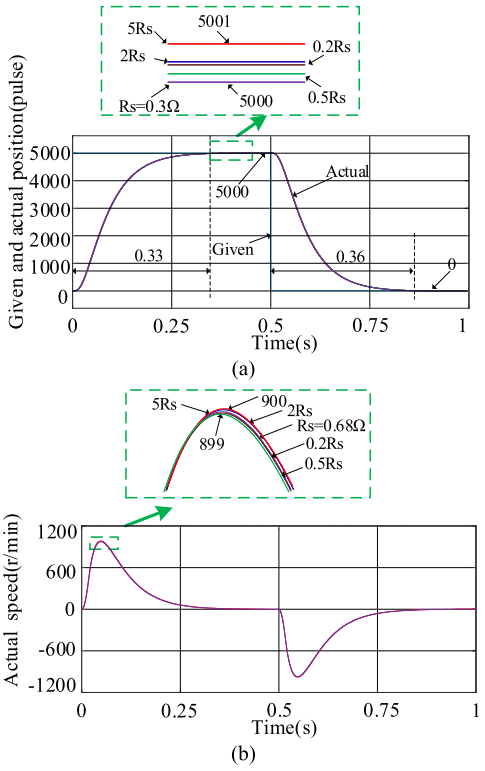

FIGURE 20. The waveform of actual position and speed under the different stator resistances. (a) The given and the actual position. (b) The actual speed.

Firstly, the influence of the stator resistance changes is analyzed. The rated value of resistance is 0.3 Ω (Rs = 0.3 Ω). When the resistance changes to 0.2 Rs, 0.5 Rs, 2 Rs, and 5 Rs, the simulation results of position and speed are as shown in Fig. 20(a) and (b), respectively. Observing the waveforms of Fig. 20(a) and (b), we can see that when 5000 pulses (as the position command) is given, the motor reaches the given position after 0.34 s and the maximum speed of the corresponding motor is 900 r/min. When the position

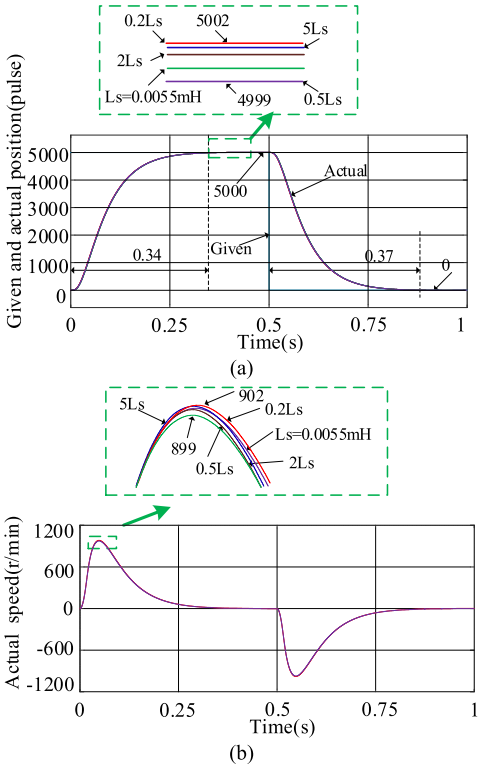

FIGURE 21. The waveform of actual position and speed under the different stator inductance. (a) The given and the actual position. (b) The actual speed.

reference is changed to 0 pulses, the motor reaches the given position after 0.36 s and the maximum speed of the corresponding motor is −900 r/min. The actual position is slightly affected by the change in the resistance, and the maximum change of the position is 1 pulse due to resistance variation. And when the resistance changes between (0.2-5) Rs, the actual speed is less affected, and the maximum speed deviation is 1 r/min. According to the above analysis, the change of resistance has little influence on the proposed FS.

Secondly, the influence of the inductance change is analyzed. The rated value of inductance is 0.0055 mH (Ls = 0.0055 mH). When the inductance value changes to 0.2 Ls, 0.5 Ls, 2 Ls, and 5 Ls, the simulation results of position and speed are as shown in Fig. 21(a) and (b), respectively. Observing the waveforms of Fig. 21(a) and (b), we can see that when 5000 pulses are given as the position reference, the motor reaches the given position after 0.34 s, and the maximum speed of the corresponding motor is 900 r/min. When the position reference is changed to 0 pulses, the motor reaches the given position after 0.37 s, and the speed of the corresponding motor is −900 r/min. The actual position is slightly affected by the change of the inductance, and the maximum position deviation is 3 pulses. And when the inductance changes between (0.2-5) Ls, the speed is less affected, and the maximum speed deviation is 4 r/min. According to the above analysis, the change of the inductance has little influence on the proposed FS.

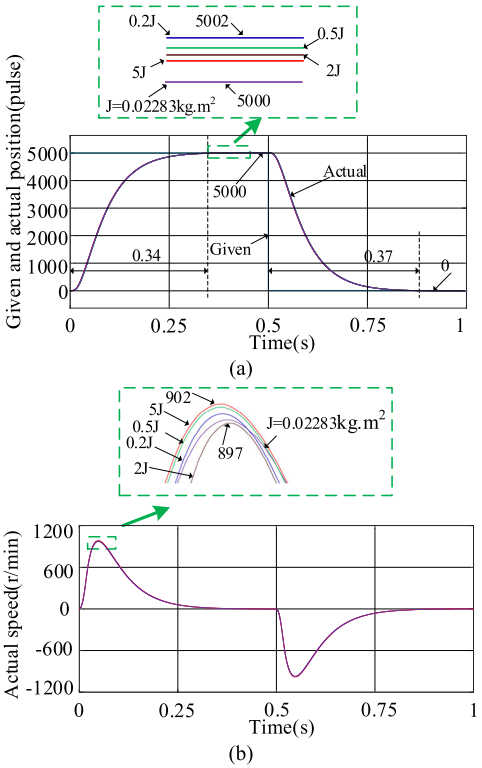

FIGURE 22. The waveform of actual position and speed under the different moment of inertia. (a) The given and the actual position. (b) The actual speed.

Finally, the influence of the change of the moment of inertia is analyzed. The rated moment of inertia of the motor is 0.02283 kg.m^2 (J = 0.02283 kg.m^2). When the moment of inertia changes to 0.2 J, 0.5 J, 2 J, and 5 J, the simulation results of position and speed are as shown in Fig. 22(a) and (b), respectively. Observing the waveforms of Fig. 22(a) and (b), we can see that when 5000 pulses are given as the position reference, the motor reaches the given position after 0.34 s, and the maximum speed of the corresponding motor is 900 r/min. When the position reference is changed to 0 pulses, the motor reaches the given position after 0.37 s, and the maximum speed of the corresponding motor is −900 r/min. The actual position is slightly affected by the change of the moment of inertia, and the maximum position deviation is 2 pulses. And when the moment of inertia changes between (0.2-5) J, the actual speed is less affected, and the maximum speed deviation is 5 r/min. According to the above analysis, the change of moment of inertia has little influence on the proposed FS.

Therefore, it can be concluded that the changes of resistance, inductance, and moment of inertia have little influence on the proposed scheme, which indicates the method has good robustness.

According to the above experimental results, the performance index of the proposed control scheme can be obtained from the experimental data, as shown in Table 4. And the results show that the proposed control scheme has the advantages of fast positioning response, high positioning accuracy, and good robustness.

TABLE 4. Performance index.

Given conditions	Rise time(s)	Descent time(s)	Positioning error(pulse)
5000 pulses, 0 N.m	0.4	0.38	0
10000 pulses,0 N.m	0.6	0.57	0
20000 pulses, 0 N.m	0.82	0.8	0
5000 pulses, 0.32 N.m	0.41	0.39	0
10000 pulses, 0.32 N.m	0.62	0.61	±1
20000 pulses, 0.32 N.m	0.83	0.81	±2

VI. CONCLUSION

In order to improve the positioning response and positioning accuracy of the manipulator joint drive system, and reduce the influence of load change on the positioning performance, a new load adaptive two-loop driving system of the manipulator's joint based on the improved position-speed integrated ADRC with the parameter fuzzy self-tuning method is proposed. In order to verify the effectiveness of the method, the driving ability of the x-axis joint drive system under different given positions and sudden load is tested. The experimental results show that the load adaptive drive system based on the proposed improved position-speed integrated ADRC without the parameter fuzzy self-tuning method has a faster positioning response than the traditional position-speed-current three-loop ADRC system, but when the load suddenly increases, the positioning error both appears. However, after the integration of the proposed parameter fuzzy self-tuning method, the influence of load disturbance is effectively suppressed, and the positioning response and positioning accuracy of the system are improved. And the proposed scheme is robust to the change of load, inductance, resistance, and inertia of PMSM. The proposed load adaptive drive system has better positioning accuracy, positioning speed, and robustness, but the speed control performance is relatively poor. Therefore, the proposed control scheme is suitable for point-to-point control occasions that do not require high-speed performance. For trajectory control occasions that require high-speed performance, it may not suitable and further optimization of the algorithm is needed.

REFERENCES

[1] F. G. Rossomando and C. M. Soria, "Adaptive neural sliding mode control in discrete time for a SCARA robot arm," *IEEE Latin Amer. Trans.*, vol. 14, no. 6, pp. 2556–2564, Jun. 2016.

[2] A. Apte, U. Thakar, and V. Joshi, "Disturbance observer based speed control of PMSM using fractional order PI controller," *IEEE/CAA J. Automatica Sinica*, vol. 6, no. 1, pp. 316–326, Jan. 2019.

[3] Y. Yan, J. Yang, Z. Sun, C. Zhang, S. Li, and H. Yu, "Robust speed regulation for PMSM servo system with multiple sources of disturbances via an augmented disturbance observer," *IEEE/ASME Trans. Mechatronics*, vol. 23, no. 2, pp. 769–780, Apr. 2018.

[4] L. He, F. Wang, J. Wang, and J. Rodriguez, "Zynq implemented luenberger disturbance observer based predictive control scheme for PMSM drives," *IEEE Trans. Power Electron.*, vol. 35, no. 2, pp. 1770–1778, Feb. 2020.

[5] L. Sheng, G. Xiaojie, and Z. Lanyong, "Robust adaptive backstepping sliding mode control for six-phase permanent magnet synchronous motor using recurrent wavelet fuzzy neural network," *IEEE Access*, vol. 5, pp. 14502–14515, 2017.

[6] P. Mani, R. Rajan, L. Shanmugam, and Y. H. Joo, "Adaptive fractional fuzzy integral sliding mode control for PMSM model," *IEEE Trans. Fuzzy Syst.*, vol. 27, no. 8, pp. 1674–1686, Aug. 2019.

[7] C. Wang and Z. Q. Zhu, "Fuzzy logic speed control of permanent magnet synchronous machine and feedback voltage ripple reduction in flux-weakening operation region," *IEEE Trans. Ind. Appl.*, vol. 56, no. 2, pp. 1505–1517, Mar. 2020.

[8] Y. Wang, Y. Feng, X. Zhang, and J. Liang, "A new reaching law for antidisturbance sliding-mode control of PMSM speed regulation system," *IEEE Trans. Power Electron.*, vol. 35, no. 4, pp. 4117–4126, Apr. 2020.

[9] Z. Ping, T. Wang, Y. Huang, H. Wang, J.-G. Lu, and Y. Li, "Internal model control of PMSM position servo system: Theory and experimental results," *IEEE Trans. Ind. Informat.*, vol. 16, no. 4, pp. 2202–2211, Apr. 2020.

[10] Y. Tuo, Y. Wang, and S. Wang, "Reliability-based robust online constructive fuzzy positioning control of a turret-moored floating production storage and offloading vessel," *IEEE Access*, vol. 6, pp. 36019–36030, 2018.

[11] H. Hu, X. Wang, and L. Chen, "Impedance sliding mode control with adaptive fuzzy compensation for robot-environment interacting," *IEEE Access*, vol. 8, pp. 19880–19889, 2020.

[12] J. Liu, H. Li, and Y. Deng, "Torque ripple minimization of PMSM based on robust ILC via adaptive sliding mode control," *IEEE Trans. Power Electron.*, vol. 33, no. 4, pp. 3655–3671, Apr. 2018.

[13] W. Lu, Z. Zhang, D. Wang, K. Lu, D. Wu, K. Ji, and L. Guo, "A new load torque identification sliding mode observer for permanent magnet synchronous machine drive system," *IEEE Trans. Power Electron.*, vol. 34, no. 8, pp. 7852–7862, Aug. 2019.

[14] A. Hezzi, S. B. Elghali, Z. Zhou, E. Elbouchikhi, and M. Benbouzid, "Linear ADRC for speed control of 5-Phase PMSM-based electric vehicles," in *Proc. Int. Conf. Electr. Inf. Technol. (ICEIT)*, Mar. 2020, pp. 1–6.

[15] S. Wang, H. Zhu, M. Wu, and W. Zhang, "Active disturbance rejection decoupling control for three-degree-of- freedom six-pole active magnetic bearing based on BP neural network," *IEEE Trans. Appl. Supercond.*, vol. 30, no. 4, pp. 1–5, Jun. 2020.

[16] C. Du, Z. Yin, Y. Zhang, J. Liu, X. Sun, and Y. Zhong, "Research on active disturbance rejection control with parameter autotune mechanism for induction motors based on adaptive particle swarm optimization algorithm with dynamic inertia weight," *IEEE Trans. Power Electron.*, vol. 34, no. 3, pp. 2841–2855, Mar. 2019.

[17] M. S. Mubarok and T.-H. Liu, "Implementation of predictive controllers for matrix-converter-based interior permanent magnet synchronous motor position control systems," *IEEE J. Emerg. Sel. Topics Power Electron.*, vol. 7, no. 1, pp. 261–273, Mar. 2019.

[18] Z. Yin, L. Gong, C. Du, J. Liu, and Y. Zhong, "Integrated position and speed loops under sliding-mode control optimized by differential evolution algorithm for PMSM drives," *IEEE Trans. Power Electron.*, vol. 34, no. 9, pp. 8994–9005, Sep. 2019.

[19] S. Ding, W.-H. Chen, K. Mei, and D. J. Murray-Smith, "Disturbance observer design for nonlinear systems represented by input–output models," *IEEE Trans. Ind. Electron.*, vol. 67, no. 2, pp. 1222–1232, Feb. 2020.

[20] Q. Hou, S. Ding, and X. Yu, "Composite super-twisting sliding mode control design for PMSM speed regulation problem based on a novel disturbance observer," *IEEE Trans. Energy Convers.*, early access, Apr. 6, 2020, doi: 10.1109/TEC.2020.2985054.

[21] D. T. Tran, D. X. Ba, and K. K. Ahn, "Adaptive backstepping sliding mode control for equilibrium position tracking of an electrohydraulic elastic manipulator," *IEEE Trans. Ind. Electron.*, vol. 67, no. 5, pp. 3860–3869, May 2020.

[22] M. Ran, Q. Wang, and C. Dong, "Active disturbance rejection control for uncertain nonaffine-in-control nonlinear systems," *IEEE Trans. Autom. Control*, vol. 62, no. 11, pp. 5830–5836, Nov. 2017.

[23] N. Peng, Y. Bai, H. Luo, and J. Bai, "Artillery position control through auto disturbance rejection controller based on fuzzy control," in *Proc. 5th Int. Conf. Intell. Hum.-Mach. Syst. Cybern.*, Aug. 2013, pp. 496–499.

[24] X. Zhou, M. Liu, Y. Ma, and S. Wen, "Improved linear active disturbance rejection controller control considering bus voltage filtering in permanent magnet synchronous generator," *IEEE Access*, vol. 8, pp. 19982–19996, 2020.

[25] H. Sira-Ramírez, J. Linares-Flores, C. García-Rodríguez, and M. Antonio Contreras-Ordaz, "On the control of the permanent magnet synchronous motor: An active disturbance rejection control approach," *IEEE Trans. Control Syst. Technol.*, vol. 22, no. 5, pp. 2056–2063, Sep. 2014.

WENQI LU (Member, IEEE) received the B.S. degree from Zhejiang Ocean University, Zhejiang, China, in 2005, and the Ph.D. degree from the Nanjing University of Aeronautics and Astronautics, Nanjing, China, in 2011.

From 2014 to 2017, he was a Postdoctoral Researcher with the Department of Electrical Engineering, Zhejiang University. From 2017 to 2018, he was a Guest Researcher with the Department of Energy Technology, Aalborg University. He is currently an Associate Professor with the Faculty of Mechanical Engineering and Automation, Zhejiang Sci-Tech University. His current research interests include the control of electric machines and mechatronic system and their application in robot, and intelligent manufacturing equipment.

QIANG LI received the B.S. degree in mechanical and electronic engineering from Quzhou University, in 2018. He is currently pursuing the M.Eng. degree in mechanical and electronic engineering with Zhejiang Sci-Tech University, Hangzhou, China. His research interests include electrical motor drives and design of the permanent magnet ac servo system for the robot.

KAIYUAN LU (Member, IEEE) received the B.S. and M.S. degrees from Zhejiang University, Zhejiang, China, in 1997 and 2000, respectively, and the Ph.D. degree from Aalborg University, Aalborg, Denmark, in 2005. In 2005, he was an Assistant Professor with the Department of Energy Technology, Aalborg University, where he has been an Associate Professor, since 2008. His research interests include the design of permanent magnet machines, FEM analysis, and control of permanent magnet machines.

YUJUN LU received the B.S. degree from Liaoning Technical University, Liaoning, China, in 2002, and the Ph.D. degree from Zhejiang University, Hangzhou, China, in 2007.

From 2011 to 2012, he was a Visiting Scholar with the FAMU-FSU College of Engineering, Florida State University. He is currently a Professor and Assistant Dean of the Faculty of Mechanical Engineering and Automation, Zhejiang Sci-Tech University. His current research interests include the mechatronic system digital design, manufacturing, and its application in intelligent manufacturing equipment.

LIANG GUO received the master's degree from Shandong University, Jinan, China, in 2003, and the Ph.D. degree from Zhejiang University, Hangzhou, China, in 2006. She was a Visiting Scholar with the Power Electronics and Machines Group, University of Nottingham, Nottingham, U.K. She is currently an Associate Professor with the Faculty of Mechanical Engineering and Automation, Zhejiang Sci-Tech University. Her current research interests include electromagnetic analysis and optimization of the electrical machine, in particular, and in permanent magnet machines.

WEICAN YAN received the B.S. and M.S. degrees from Zhejiang University, Zhejiang, China, in 1990 and 2005, respectively, where he is currently pursuing the Ph.D. degree. Since 1990, he has been engaged in motor and control technology and product development and management with Wolong Electric Group Company Ltd. His research interests include the design and application of high-efficiency motor, and drive and motor systems.

FENG XU received the master's degree in materials processing engineering from the Shaanxi University of Science and Technology, Xi'an, Shanxi, China, in 2007. He is currently a Mechanical Expert with Maider Medical Industry Equipment Company Ltd. His current research interests include the cam mechanism, medical disposable automatic assembly equipment, and tobacco packaging machinery.